Supplement of Atmos. Chem. Phys., 20, 4399–4414, 2020
https://doi.org/10.5194/acp-20-4399-2020-supplement
© Author(s) 2020. This work is distributed under
the Creative Commons Attribution 4.0 License.

Atmospheric Chemistry and Physics
Open Access
EGU

*Supplement of*

# Ozone pollution over China and India: seasonality and sources

**Meng Gao et al.**

*Correspondence to:* Meng Gao (mmgao2@hkbu.edu.hk) and Michael B. McElroy (mbm@seas.harvard.edu)

The copyright of individual parts of the supplement might differ from the CC BY 4.0 License.

**Supplemental Information**

Table S1 Selected physics configuration options

| Feature | Option | Description |
|---|---|---|
| Microphysics | Lin scheme | Lin et al., 1983 |
| Long-wave Radiation | Rapid Radiative Transfer Model (RRTM) | Mlawer et al., 1997 |
| Shortwave Radiation | Goddard shortwave | Chou et al., 1998 |
| Surface Model | Noah Land | Ek et al., 2003 |
| Planetary boundary layer parameterization | Yonsei University | Hong et al., 2006 |


Chou, M.-D., Suarez, M. J., Ho, C.-H., Yan, M. M.-H. and Lee, K.-T.: Parameterizations for cloud overlapping and shortwave single-scattering properties for use in general circulation and cloud ensemble models, J. Climate, 11, 202–214, 1998.

Ek, M.B., Mitchell, K.E., Lin, Y., Rogers, E., Grunmann, P., Koren, V., Gayno, G. and Tarpley, J.D.: Implementation of Noah land surface model advances in the National Centers for Environmental Prediction operational mesoscale Eta model. J. Geophys. Res., 108(D22), 2003.

Hong, S.-Y., Noh, Y., and Dudhia, J.: A New Vertical Diffusion Package with an Explicit Treatment of Entrainment Processes, Mon. Weather Rev., 134, 2318–2341, 2006.

Lin, Y.-L., Farley, R. D., and Orville, H. D.: Bulk parameterization of the snow field in a cloud model, J. Clim. Appl. Meteorol., 22, 1065–1092, 1983.

Mlawer, E. J., Taubman, S. J., Brown, P. D., Iacono, M. J., and Clough, S. A.: Radiative transfer for inhomogeneous atmospheres: RRTM, a validated correlated-k model for the longwave, J. Geophys. Res., 102, 16663–16682, doi:10.1029/97JD00237, 1997.

Table S2 Amount of emission species from anthropogenic, biogenic and biomass burning sources (Tg/year)

| China | $SO_2$ | $NO_x$ | NMVOC | $NH_3$ | CO | $PM_{2.5}$ | BC | OC |
|---|---|---|---|---|---|---|---|---|
| Anthropogenic | 28.5 | 29.2 | 28.1 | 10.7 | 180.2 | 11.9 | 1.8 | 3.2 |
| Biogenic | | 0.3 | 24 | | 2.9 | | | |
| Biomass burning | 0.2 | 0.2 | 0.6 | 0.1 | 6.7 | 0.6 | 0.04 | 0.3 |
| India | | | | | | | | |
| Anthropogenic | 8.4 | 8.9 | 16.0 | 9.4 | 61.8 | 4.9 | 1.0 | 2.5 |
| Biogenic | | 0.3 | 18.7 | | 2.7 | | | |
| Biomass burning | 0.1 | 0.7 | 0.8 | 0.2 | 18.5 | 1.9 | 0.1 | 0.9 |

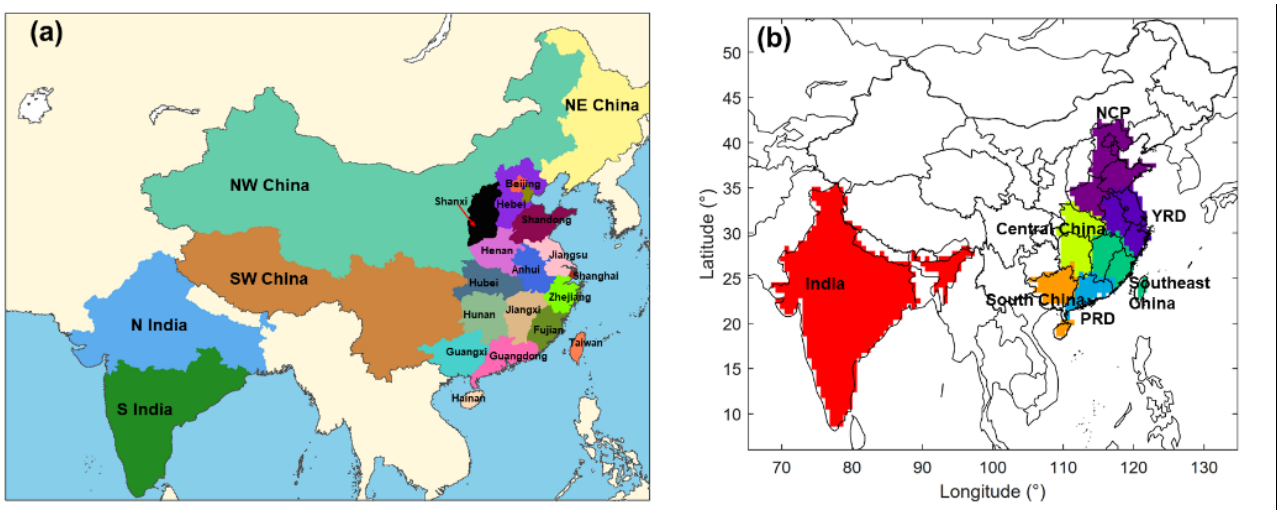


Figure S1. Source regions are marked in different colors.

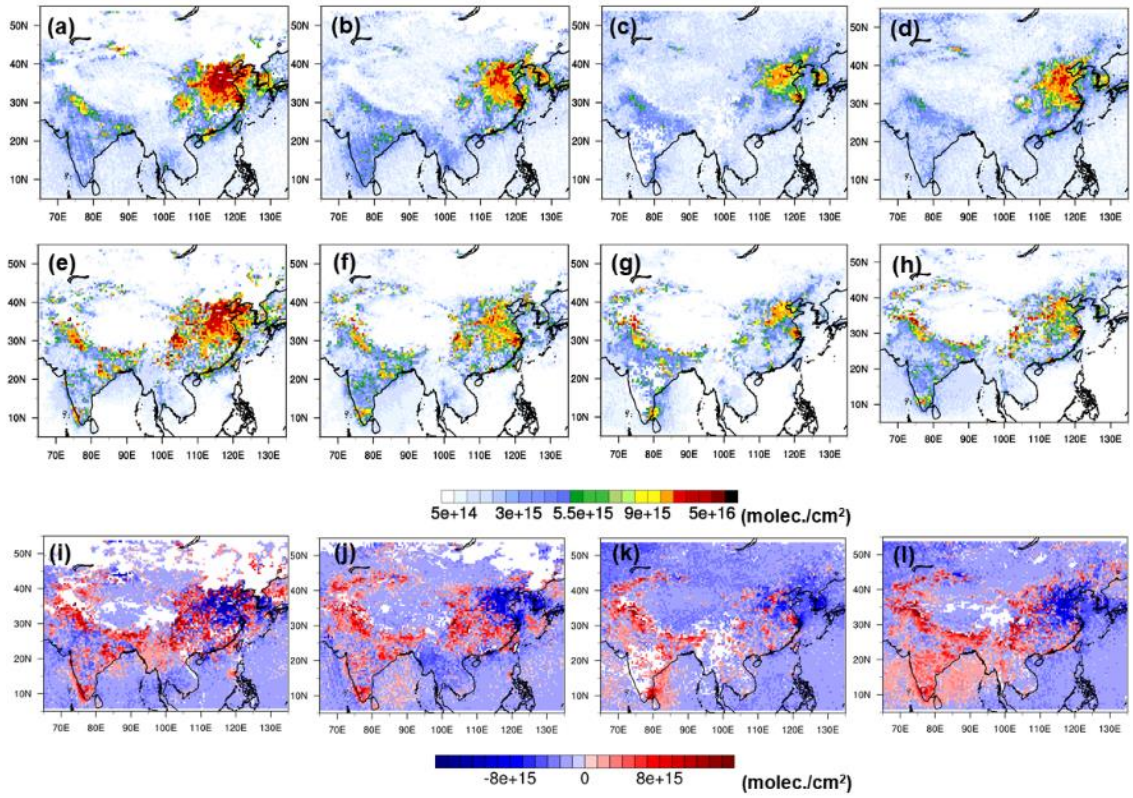


Figure S2. Observed and WRF-Chem modeled $NO_2$ column and their differences (model minus observation) for winter (a, e, i), spring (b, f, j), summer (c, g, k) and autumn (d, h, l).

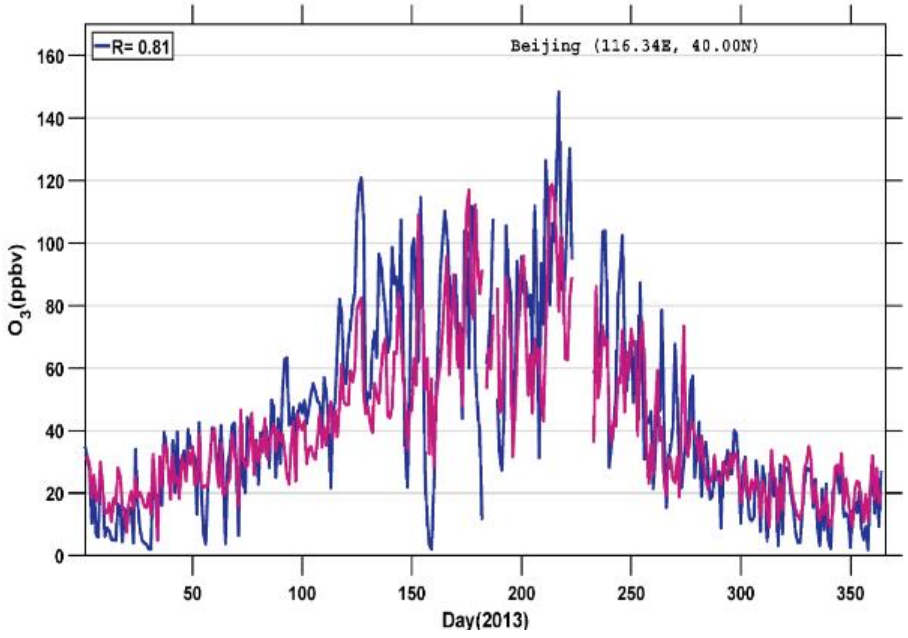


Figure S3. Observed (blue) and Modeled (red) daily maximum 8-hr average ozone in Beijing.

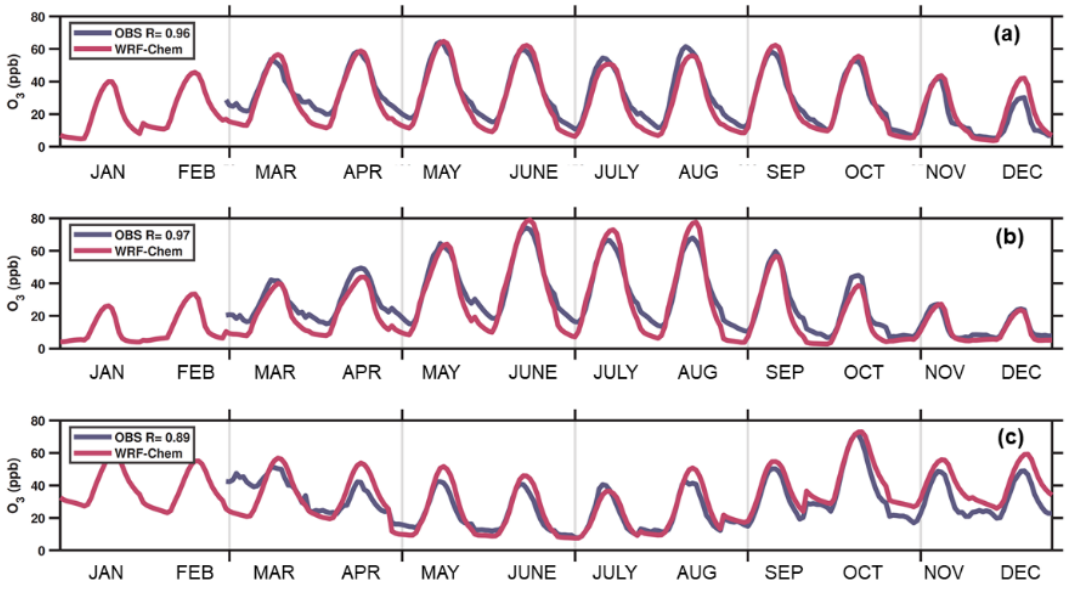


Figure S4. Comparison between observed (blue) and modeled (red) monthly averaged diurnal variations of $O_3$ concentrations in the NCP (a), YRD (b) and PRD (c).

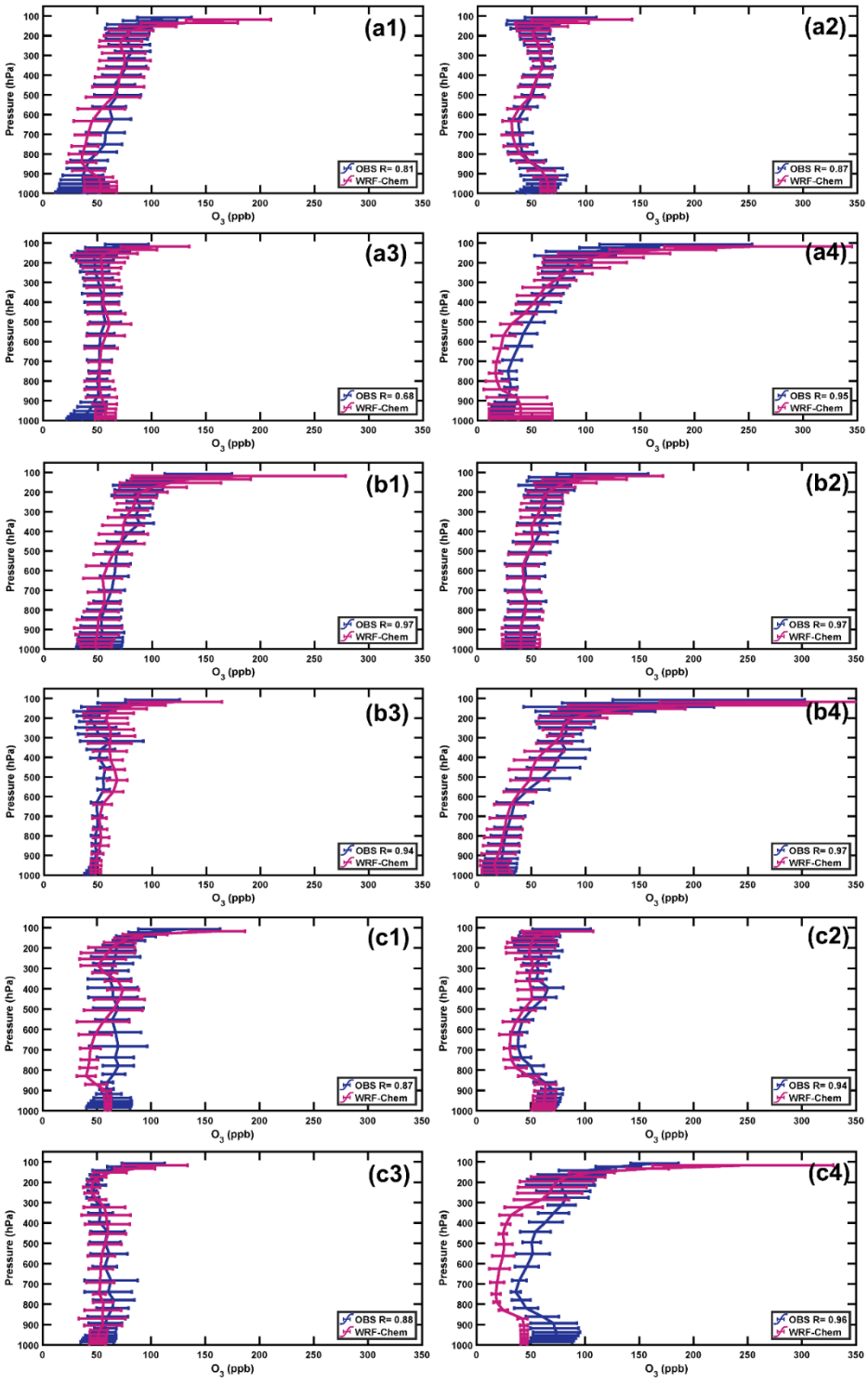


Figure S5. Observed and simulated seasonal mean $O_3$ concentrations for the HKO (Hong Kong Observatory, a1-a4), JMA (Japan Meteorological Agency, b1-b4), and HSSRV (Hydrometeorological Service of S.R. Vietnam, c1-c4) stations.

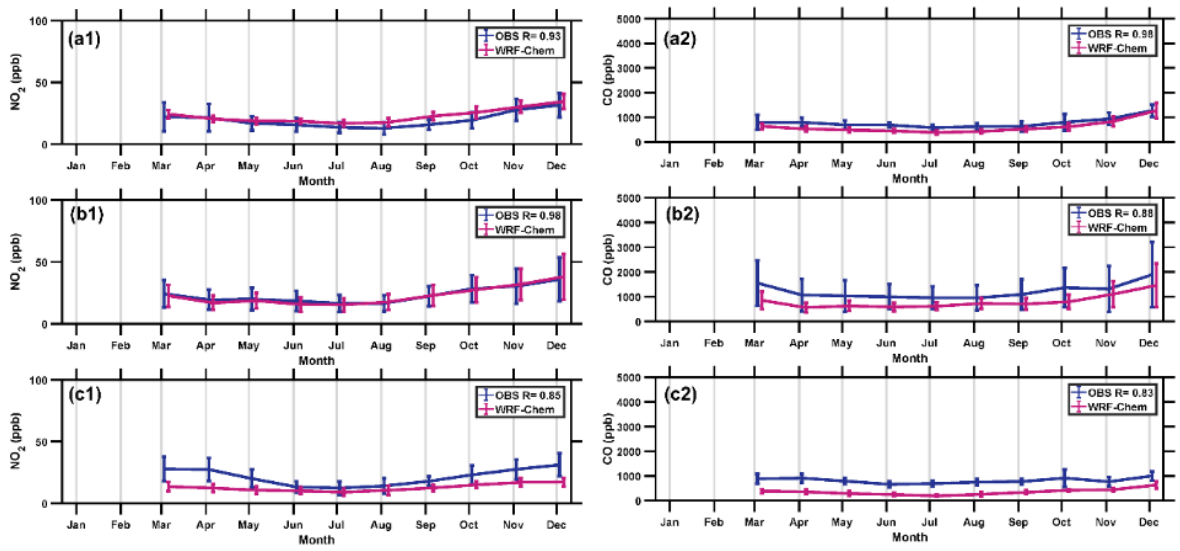


Figure S6. Modeled and observed monthly concentrations of $NO_2$ and CO in NCP (a1-a2), YRD (b1-b2), and PRD (c1-c2).

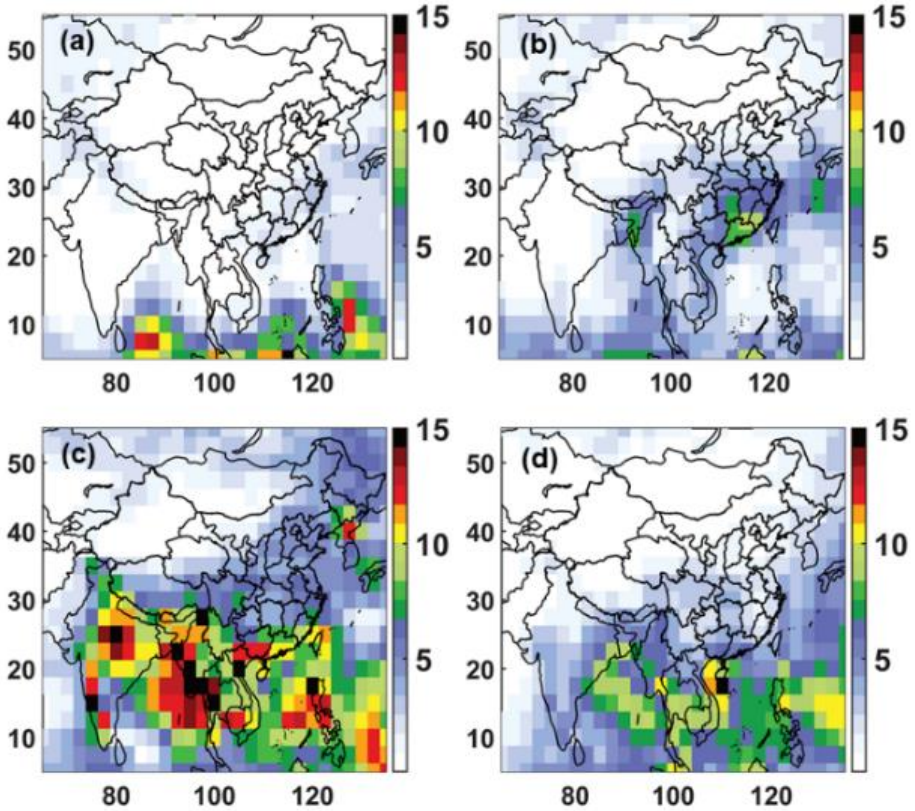


Figure S7. Mean precipitation (mm/day) in DJF (a), MAM (b), JJA (c) and SON (d) inferred from the Global Precipitation Climatology Project (GPCP) version 2.3 dataset.

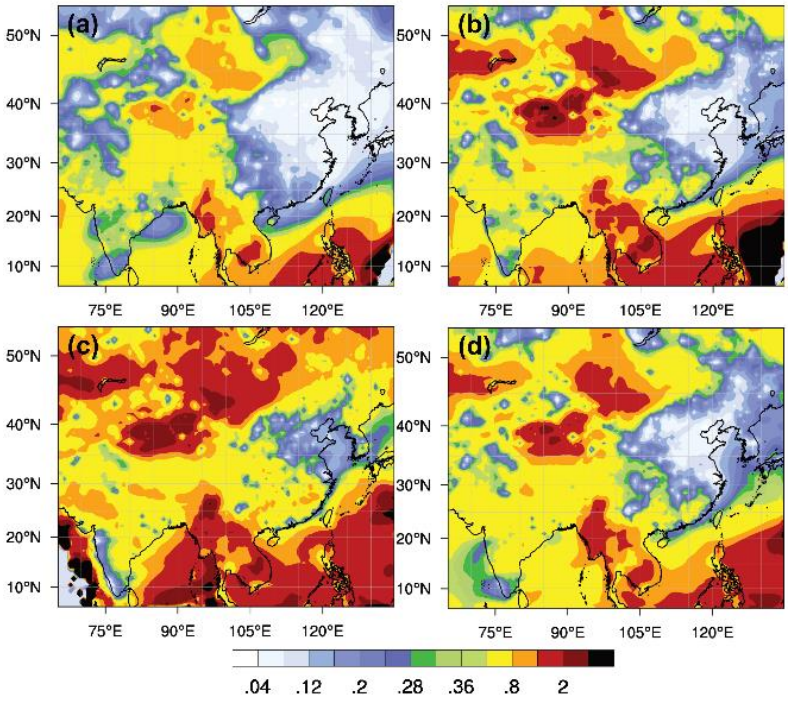


Figure S8. WRF-Chem simulated mean ratios of HCHO to $NO_y$ for DJF (a), MAM (b), JJA (c) and SON (d).

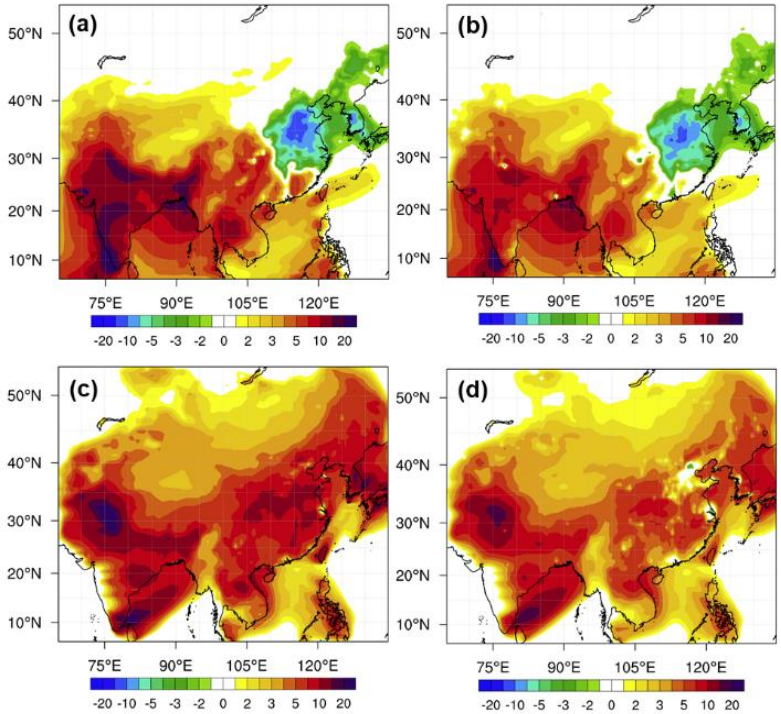


Figure S9. Distributions of the contributions of transportation sector to daytime (a, c) and daily (c, d) mean concentrations of $O_3$ in February and July.

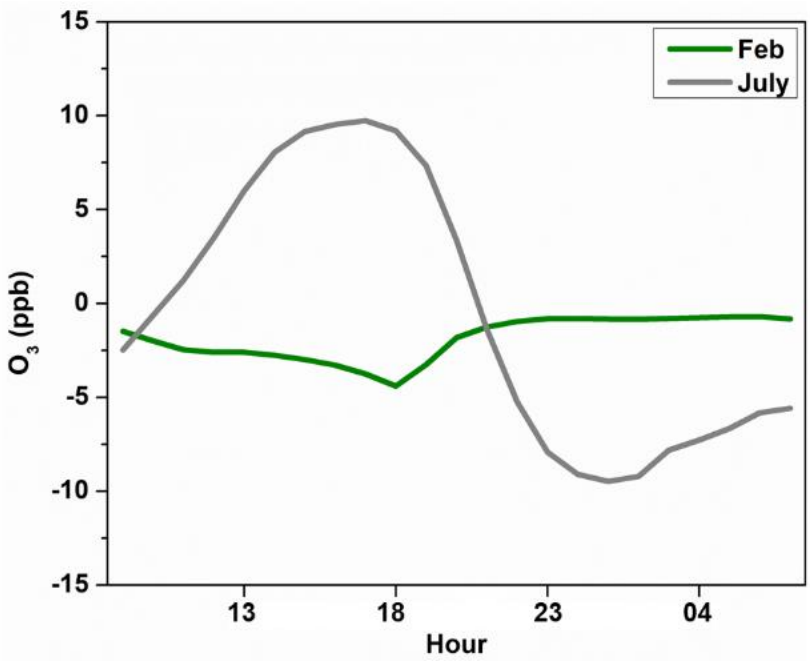


Figure S10. Diurnal features of $O_3$ sensitivity to transportation sector in Beijing in February in July.